# Effect of Screw Distribution on the Structural Response and Buckling Behavior of Built-Up Cold-Formed Steel Columns

Zamzami Septiropa[1,*], Abi Mufid Octavio[2], Achmad Fauzan Hery Soegiharto[2], Arizu Sulaiman[3]

[1]Department of Civil Engineering, University of Muhammadiyah Malang, Malang, Indonesia

[2]Department of Mechanical Engineering, University of Muhammadiyah Malang, Malang, Indonesia

[3]School of Civil Engineering, University of Technology Malaysia, Johor Bahru, Malaysia

Received 29 July 2026; revised 21 October 2026; accepted 22 October 2026

DOI: https://doi.org/10.46604/peti.2026.16660

## Abstract

Built-up cold-formed steel (CFS) columns offer a high strength-to-weight ratio, but the influence of screw distribution on elastic response and buckling behavior remains insufficiently understood. This study investigates five screw distributions (S50–S90) in double back-to-back (dBB) and double flange-to-flange (dFF) columns using finite element analysis and experimental compression tests. Six self-drilling screws and a column length of 500 mm are maintained, so screw spacing and end distance vary simultaneously. In dBB, equivalent elastic strain and stress vary by 22.31% and 22.94%, respectively, compared with 2.64% and 6.82% in dFF. The buckling load factor (BLF) varies by 7.11% for dBB and 3.22% for dFF, indicating greater sensitivity to screw distribution. S60 produces the highest BLF for dBB (2.4774), whereas S80 produces the highest for dFF (3.3173). These findings demonstrate that profile orientation influences structural response and relative elastic buckling stability. The BLF indicates comparative elastic stability, not actual ultimate compression capacity.

**Keywords:** built-up cold-formed steel, screw distribution, finite element analysis, buckling behavior

## 1. Introduction

Cold-formed steel (CFS) is a widely used structural material in modern construction. This material offers a high strength-to-weight ratio, a simple fabrication process, and cost and time efficiency during installation [1]. The mechanical properties of steel also play an important role in determining the structural response of steel components under mechanical loading [2]. Various applications, such as industrial buildings, warehouses, roof trusses, and modular construction systems, have utilized CFS profiles as primary structural elements [3]. However, the thin-walled nature of CFS profiles increases their susceptibility to buckling when subjected to axial compressive loads [4]. Structural failure is typically preceded by local buckling, distortional buckling, or global buckling before the material reaches its yield stress [5]. Stress concentration and localized structural defects can also contribute to progressive damage and failure in steel structures [6]. Consequently, the compressive capacity of a single profile is limited.

One widely adopted approach to increasing the compressive capacity of CFS profiles is to form a built-up section. This approach involves joining two or more profiles using self-drilling screw connections [7]. The built-up configuration increases the section's moment of inertia and stiffness. Furthermore, the interaction between profiles creates a composite action that enhances the structure's axial capacity and stability. However, the effectiveness of the composite action is significantly influenced by the joint configuration. Additionally, the distribution and spacing of the screws determine the effectiveness of force transfer among the constituent profiles.

* Corresponding author. E-mail address: zamseptiropa@umm.ac.id

Previous studies have examined built-up cold-formed steel (CFS) members and their screw connections from both structural and connection-level perspectives. Experimental tests and numerical parametric analyses of back-to-back built-up CFS columns have shown that fastener spacing and the shear-resistance characteristics of connections influence flexural buckling behavior and load-bearing capacity [8]. Research on screwed connections has also examined their shear behavior and capacity at ambient and elevated temperatures, highlighting the importance of connection-level performance in built-up CFS members [9]. More recently, experimental testing and numerical simulations have been used to investigate the axial compression behavior and failure mechanisms of screw-connected built-up CFS members [10]. In addition, monotonic tests of 225 steel-to-steel screw connections have supported the development of a shear-slip constitutive model for numerical analysis of built-up back-to-back CFS columns [11]. Collectively, these studies demonstrate that the structural response of built-up CFS members depends on the interaction between the constituent profiles, the mechanical behavior of the connections, and the arrangement of the fasteners.

More specifically, Septiropa et al. investigated the effect of screw distance on the compression capacity of combined CFS profiles. Their results showed similar responses for screw spacings of 25, 50, and 75 mm, whereas larger spacings of 100, 125, and 150 mm produced lower capacities. However, the number of screws also varied among the specimens, making it difficult to isolate the effect of screw spacing from that of connector quantity [12]. Deniziak et al. examined the influence of interconnecting bolt spacing on stress distribution and compressive resistance. Their study increased the bolt-series spacing from 450 to 650 mm, corresponding to an increase of approximately 44%. The increased spacing had a limited effect on load-bearing resistance, while the built-up columns exhibited an average axial compression resistance 35% higher than that of a single-chord column [13].

Suhaib and Tantray investigated the flexural behavior of built-up CFS beams with different screw arrangements. Their experimental results showed reductions in ultimate moment capacity of 6.18%, 3.54%, and 2.90% when longitudinal screw spacing increased from 150 to 275 mm for one, two, and three screw rows, respectively. Their numerical study further examined 124 beam models with four web depths. For the single-row screw arrangement, increasing the spacing from 50 to 1050 mm reduced moment capacity by 11%, 14%, 17%, and 19% for web depths of 150, 200, 250, and 300 mm, respectively. A similar decreasing trend was observed for configurations with two and three screw rows [14].

These limitations are also evident in the parameters evaluated in previous studies. Most studies have focused primarily on ultimate capacities obtained from testing. Analysis of structural response mechanisms remains limited. The relationship between screw distribution, elastic deformation, stress distribution, strain redistribution, and buckling resistance has not yet been comprehensively explained. However, understanding these mechanisms is crucial for identifying more efficient joint configurations in built-up cold-formed steel members.

Accordingly, this study investigates the influence of overall screw distribution on the elastic response and buckling behavior of built-up cold-formed steel (CFS) columns using a finite element model validated against experimental results. Five configurations (S50–S90) are evaluated for double back-to-back (dBB) and double flange-to-flange (dFF) columns, with six screws and a column length of 500 mm maintained in all models. Because screw spacing and end distance vary simultaneously, the investigated parameter represents overall screw distribution rather than screw spacing alone.

Static structural analysis evaluates total deformation, equivalent elastic strain, and equivalent stress [15]. Furthermore, eigenvalue buckling analysis determines the buckling load factor (BLF), the corresponding elastic eigenvalue buckling load, and buckling modes to compare relative elastic buckling stability [16]. The main contribution of this study is a controlled comparison of how overall connection layout affects internal elastic response and relative buckling stability in two built-up column orientations, without treating eigenvalue buckling loads as predictions of actual ultimate compression capacity.

## 2. Research Methodology

### *2.1 Specimen configuration*

This study uses C-lipped cold-formed steel (CFS) profiles to construct built-up columns. The profile geometry follows the experimental specimens reported by Septiropa et al. [12]. The cross-sectional geometry is illustrated in Fig. 1, and the geometric dimensions and specimen parameters are summarized in Table 1.

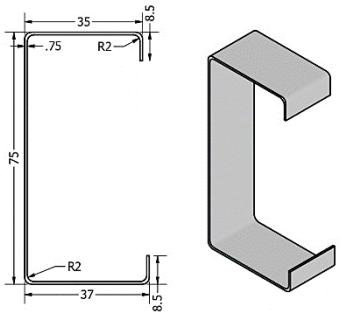



Fig. 1 Geometry and dimensions of the C-lipped cold-formed steel profile

All specimens share identical cross-sectional dimensions. The C-lipped profile has a section height of 75 mm, upper and lower flange widths of 35 and 37 mm, respectively, a lip length of 8.5 mm, and a thickness of 0.75 mm. The adopted dimensions are summarized in Table 1.

Table 1 Geometric dimensions and specimen parameters of the built-up CFS columns

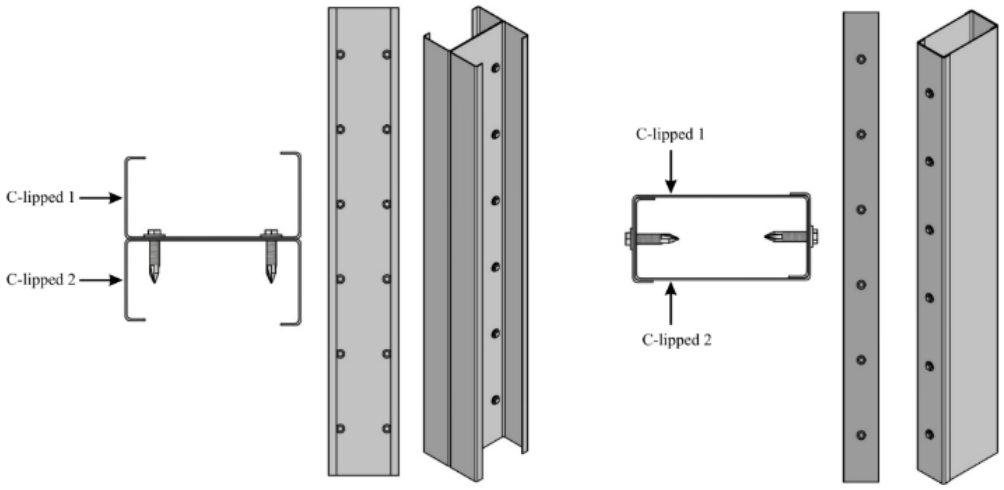
| Category | Parameter | Value | Unit |
|---|---|---|---|
| Geometry | Section height | 75 | mm |
| | Top flange width | 35 | mm |
| | Bottom flange width | 37 | mm |
| | Lip length | 8.5 | mm |
| | Thickness | 0.75 | mm |
| Specimen | Material | CFS (SS400) | – |
| | Cross-section type | C-lipped channel | – |
| | Column length | 500 | mm |
| | Number of profiles | 2 | – |
| Connection | Screw-hole diameter | 4.165 | mm |
| | Self-drilling screw length | 20 | mm |
| Configuration | Built-up arrangement | dBB and dFF | – |

This study considers two built-up configurations: double back-to-back (dBB) and double flange-to-flange (dFF). Both configurations consist of two identical C-lipped profiles, but their different orientations result in different geometric properties of the assembled sections [17]. These differences affect the principal moments of inertia, radii of gyration, and slenderness ratios, which are relevant to interpreting structural stiffness and elastic buckling behavior [18]. The geometric properties of the complete dBB and dFF sections are summarized in Table 2.

Table 2 Geometric properties of the complete built-up sections

| Property | dBB | dFF | Unit |
|---|---|---|---|
| Cross-sectional area, $A$ | 241.50 | 241.50 | mm² |
| Principal moment of inertia, $I_1$ | 223,305.911 | 223,502.956 | mm⁴ |
| Principal moment of inertia, $I_2$ | 76,139.580 | 53,012.891 | mm⁴ |
| Principal radius of gyration, $r_1$ | 30.408 | 30.422 | mm |
| Principal radius of gyration, $r_2$ | 17.756 | 14.816 | mm |
| Column length, $L$ | 500 | 500 | mm |
| Slenderness ratio, $\lambda_1 = L/r_1$ | 16.44 | 16.43 | – |
| Slenderness ratio, $\lambda_2 = L/r_2$ | 28.16 | 33.73 | – |

As shown in Fig. 2, both configurations have the same cross-sectional area because they consist of two identical profiles. However, their different orientations produce distinct sectional properties. The dFF configuration has a slightly higher $I_1$, whereas the dBB configuration has higher $I_2$ and $r_2$. Consequently, the slenderness ratio associated with $r_2$ is lower for dBB than for dFF. These geometric differences provide a basis for examining how profile orientation and overall screw distribution affect the elastic response and relative buckling stability of the assembled columns.




(a) dBB (b) dFF

Fig. 2 Cross-sectional and three-dimensional arrangements of the built-up CFS columns

*2.2 Screw distribution configuration*

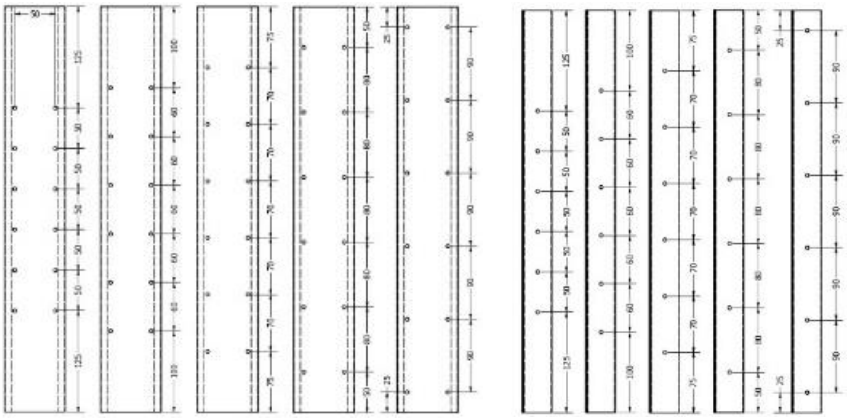
This study investigates five overall screw distribution configurations, designated S50, S60, S70, S80, and S90. Each designation represents the nominal spacing between adjacent screws. The number of screws is maintained at six, and the column length is fixed at 500 mm across all models. Consequently, increasing the screw spacing from 50 to 90 mm simultaneously reduces the end distance from 125 to 25 mm. Screw spacing and end distance therefore vary together, meaning that the study evaluates overall screw distribution rather than the isolated effect of screw spacing [19]. The configurations are summarized in Table 3.

Table 3 Screw distribution configurations adopted in this study

| Code | Number of screws | End distance (mm) | Screw spacing (mm) |
|---|---|---|---|
| S50 | 6 | 125 | 50 |
| S60 | 6 | 100 | 60 |
| S70 | 6 | 75 | 70 |
| S80 | 6 | 50 | 80 |
| S90 | 6 | 25 | 90 |

The S80 configuration corresponds to the experimental specimens used for model validation, following the experimental work reported by Septiropa et al. [12]. The remaining configurations are investigated numerically to examine the effects of different overall screw distributions. The 50–90 mm range, with increments of 10 mm, provides a systematic comparison around the S80 validation configuration while maintaining the same column length and number of screws. The screw length and screw-hole diameter are also kept constant at 20 and 4.165 mm, respectively, to maintain consistent connection dimensions across all models.

The five configurations are illustrated in Fig. 3. The schematic identifies the screw spacing, end distance, fixed column length, and number of screws, allowing the geometric differences between configurations S50–S90 to be compared directly. The same screw distribution definitions apply to both dBB and dFF configurations.



(a) dBB (b) dFF

Fig. 3 Schematic representation of the five overall screw distribution configurations (S50–S90)

### *2.3 Set up simulation*

The finite element model was developed using ANSYS Mechanical Workbench 2025 R2 to represent the built-up cold-formed steel (CFS) column under axial compression. The assembly consisted of two CFS profiles, six self-drilling screws, upper and lower steel loading plates, and a rubber sheet. The overall model, including its mesh, screw connections, loading, and boundary conditions, is presented in Fig. 4.

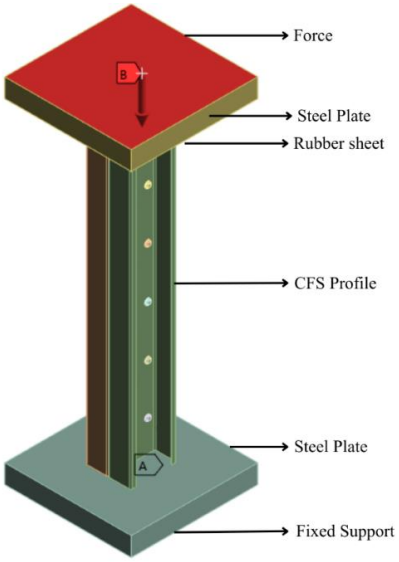



Fig. 4 Three-dimensional finite element model of the built-up CFS column

The CFS profiles were modeled as three-dimensional solid bodies using SOLID187 ten-node quadratic tetrahedral elements. The self-drilling screws were represented by cylindrical solid bodies, without explicitly modeling their threats to reduce computational complexity. The steel profiles were assigned homogeneous, isotropic, linear-elastic material behavior. The relevant elastic parameters and reference strength values are summarized in Table 4.

Table 4 Elastic material parameters and reference strength values

| Material property | Value | Unit |
|---|---|---|
| Density | 7850 | kg/m³ |
| Tensile yield strength | 597 | MPa |
| Tensile ultimate strength | 460 | MPa |
| Compressive yield strength | 250 | MPa |
| Young’s modulus | 209 | GPa |
| Poisson’s ratio | 0.30 | - |

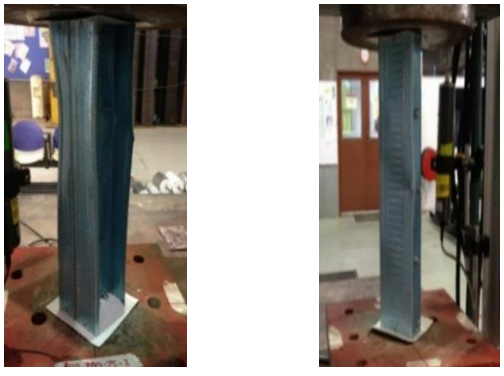
The experimental tensile properties and Young's modulus were obtained from material characterization tests on the CFS C7575 profile. The density and Poisson's ratio were adopted as standard steel parameters. The nominal compressive reference strength of 250 MPa was used separately for stress-utilization assessment and does not represent an experimentally measured compressive yield strength of the CFS profile. The screw connections were modeled using explicit screw bodies and corresponding holes in the CFS profiles. Frictional contact with an augmented Lagrange formulation was applied between the screws and surrounding steel surfaces. Frictional contact was also defined between the adjacent CFS profiles rather than assuming a bonded connection, allowing relative movement and contact pressure to develop during loading.

The loading assembly consisted of an upper steel plate, a rubber sheet, and a lower steel plate. Contact interaction was defined between the rubber sheet and adjacent steel surfaces. The lower steel plate was constrained using Fixed Support, while a compressive reference load of 20 kN was applied to the upper steel plate using Remote Force. The resulting static structural solution was transferred to the eigenvalue buckling analysis to determine the buckling load factor (BLF) and corresponding mode shape. The first positive eigenvalue was used to compare relative elastic buckling stability rather than to predict the actual ultimate compression capacity of the specimens.

Each model required approximately 30–50 min of computational time for the static structural and subsequent eigenvalue buckling analyses. Mesh sensitivity was assessed using the dBB S80 configuration. The selected 8.5 mm mesh consisted of 41,684 elements and produced a maximum equivalent stress of 157.18 MPa and a BLF of 2.3453. Compared with the 7.5 mm mesh, the maximum equivalent stress differed by approximately 0.26%, while the BLF differed by approximately 0.15%. These relatively small changes indicate that the selected mesh provides sufficiently consistent results for the subsequent parametric simulations.

### *2.4 Model validation*

Model validation was conducted using the S80 configuration for both double back-to-back (dBB) and double flange-to-flange (dFF) columns. Each configuration was tested three times under axial compression using a Tinius-Olsen universal testing machine. Fig. 5 shows the experimental loading arrangement for the two built-up configurations, with the specimens positioned vertically between the machine platens and tested under the same compression procedure.



(a) dBB (b) dFF

Fig. 5 Experimental axial compression setup for the S80 built-up CFS columns

The specimens consisted of two C-lipped CFS profiles connected by six self-drilling screws. For the S80 configuration, the screw spacing was 80 mm, the end distance was 50 mm, the screw length was 20 mm, and the screw-hole diameter was 4.165 mm. These geometric and connection parameters were reproduced in the numerical models. The material parameters assigned to the finite element model are provided in Table 4 and were kept consistent for both configurations.

The experimental peak loads from the three tests are summarized in Table 5. The dBB specimens reached peak loads of 47.32, 47.48, and 47.70 kN, giving an average of 47.50 kN. The dFF specimens reached peak loads of 67.08, 67.20, and 67.29 kN, giving an average of 67.19 kN.

Table 5 Experimental axial compression results used for model validation

| Configuration | Test 1 (kN) | Test 2 (kN) | Test 3 (kN) | Average (kN) |
|---|---|---|---|---|
| dBB (S80) | 47.32 | 47.48 | 47.70 | 47.50 |
| dFF (S80) | 67.08 | 67.20 | 67.29 | 67.19 |

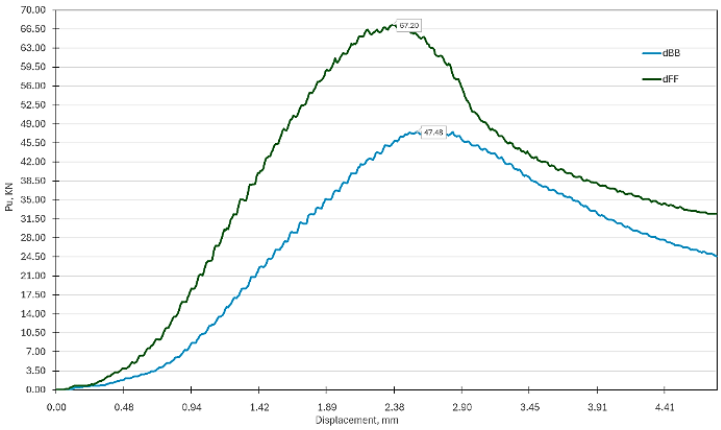



Fig. 6 Experimental load–displacement responses of the S80 specimens

The experimental load–displacement responses are presented in Fig. 6. Both configurations exhibit increasing load with axial displacement before reaching their respective peak loads, followed by a reduction in load as deformation develops. The dFF configuration sustains a higher peak load than dBB, with average loads of 67.19 and 47.50 kN, respectively. This difference reflects the structural response of the assembled configurations rather than a difference in the assigned material properties.

The load–displacement responses show that the dFF configuration sustains a higher axial load than the dBB configuration. The curves provide a direct representation of the experimental structural response and complement the comparison based on maximum load.

Following the compression tests, the specimens were examined to identify their deformation characteristics. Fig. 7 shows localized deformation in the thin-walled CFS profiles, particularly around the web and flange regions. The observed deformation is more pronounced in the dBB specimens, whereas the dFF specimens exhibit a less pronounced local deformation pattern. The screws remained engaged with the profiles, and no visible screw pull-out or complete separation of the connected profiles was observed. These observations indicate that the deformation was mainly associated with the thin-walled profiles rather than with gross failure of the screw connections.



(a) dBB (b) dFF

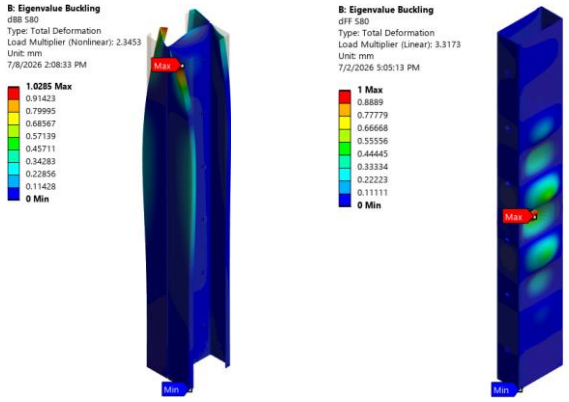
Fig. 7 Post-test deformation of the S80 specimens

For the numerical comparison, a Static structural analysis was performed under a 20 kN reference compressive load. The prestressed state was transferred to the eigenvalue buckling analysis to determine the first positive buckling load factor (BLF) and the corresponding elastic eigenvalue buckling load. The latter was calculated using the following expression [20]:

$$P_{cr} = BLF \times P_{ref} \tag{1}$$

where $P_{cr}$ is the elastic eigenvalue buckling load, BLF is the buckling load factor obtained from the eigenvalue analysis, and $P_{ref}$ is the applied reference load.

The first-mode elastic buckling shapes of the S80 numerical models are presented in Fig. 8. Both configurations exhibit predominantly local buckling, with deformation concentrated in the thin-walled plate elements rather than pronounced overall flexural deformation. The dBB configuration shows localized deformation near the upper region of the profile, whereas the dFF configuration exhibits a more distributed local deformation pattern along the connected profile.




(a) dBB (b) dFF

Fig. 8 First-mode elastic buckling shapes of the S80 numerical models

The experimental average peak loads and numerical elastic eigenvalue buckling loads are compared in Table 6. The numerical elastic buckling load for dBB is 46.906 kN, compared with the experimental average peak load of 47.50 kN. For dFF, the numerical elastic eigenvalue buckling load calculated from the BLF is 66.346 kN, compared with the experimental average peak load of 67.19 kN. The corresponding relative differences are approximately 1.251% and 1.256%, respectively.

Table 6 Comparison of experimental peak loads and numerical elastic eigenvalue buckling loads for the S80 specimens

| Configuration | Experimental average load (kN) | Numerical critical load (kN) | Difference (%) |
|---|---|---|---|
| dBB (S80) | 47.50 | 46.906 | 1.25 |
| dFF (S80) | 67.19 | 66.35 | 1.25 |

The comparison in Table 6 provides an indicative comparison of the experimental peak loads and numerical elastic eigenvalue buckling loads. These quantities have different physical meanings, and the relative differences should not be interpreted as conventional validation errors for ultimate compression capacity. Accordingly, the consistency assessment also considers the repeated experimental results, load–displacement responses, post-test deformation observations, and local buckling characteristics identified in the numerical first modes.

The present numerical analysis uses linear-elastic static structural and eigenvalue buckling analyses. It does not explicitly account for initial geometric imperfections, material yielding, large deformation, connection slip during nonlinear loading, or post-buckling behavior. Consequently, the model is used to compare relative elastic buckling stability and structural response among the investigated configurations rather than to predict the actual ultimate compression capacity. A more complete validation of ultimate capacity would require a geometrically and materially nonlinear analysis that reproduces the experimental nonlinear load–displacement response.

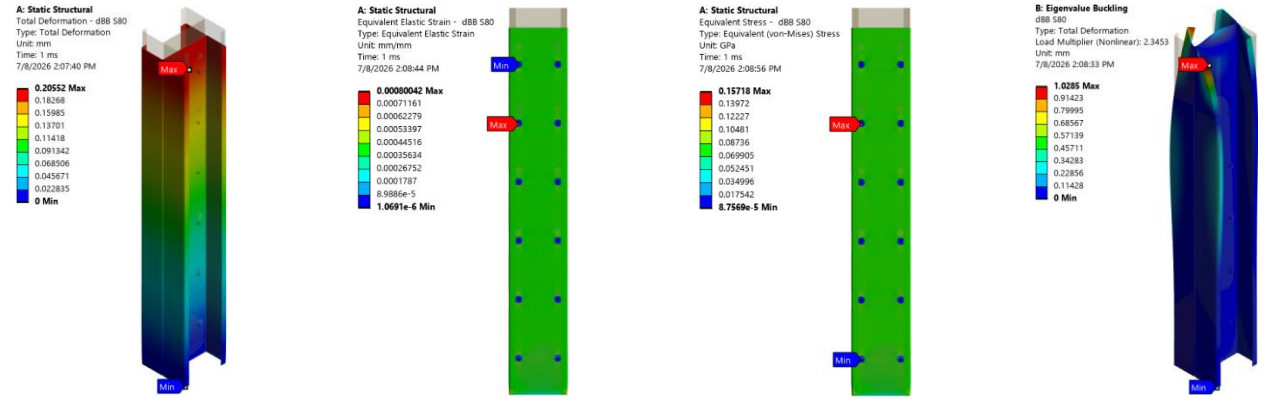
## 3. Results

Numerical simulations were conducted to investigate the effects of overall screw distribution on the structural response and elastic buckling behavior of built-up cold-formed steel columns. Five configurations (S50, S60, S70, S80, and S90) were

analyzed using static structural and eigenvalue buckling analyses. The evaluated parameters included total deformation, equivalent elastic strain, equivalent stress, and buckling load factor (BLF). All models used the same loading conditions, material properties, and boundary conditions. Differences between the dBB and dFF configurations were interpreted by considering their assembled-section geometric properties and the coupled variations in screw spacing and end distance. The results were compared to examine how overall screw distribution influences elastic deformation, internal stress and strain, and relative elastic buckling stability.

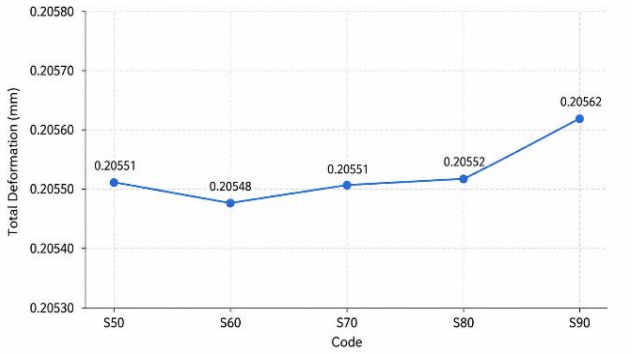
### *3.1 Structural response of double back-to-back configuration*

The simulation results for the dBB configuration are presented in Figs. 9 and 10. Static structural analysis and eigenvalue buckling analysis were used to evaluate the response of the column under different screw distributions. Fig. 9 shows the representative simulation results for the S80 configuration, including total deformation, equivalent elastic strain, equivalent stress, and the first-mode elastic buckling shape. Fig. 10 shows the changes in these responses across the five screw distribution configurations (S50-S90).

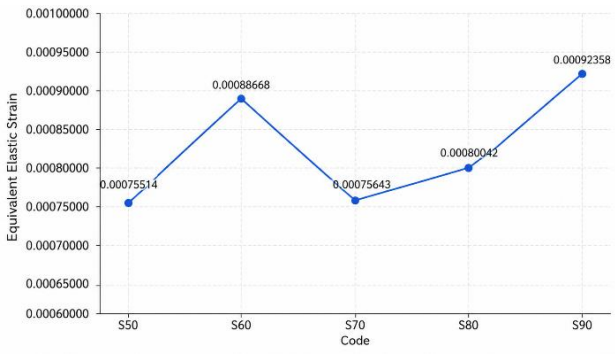



(a) Total deformation (b) Equivalent elastic strain (c) Equivalent stress (d) First-mode elastic buckling shapes

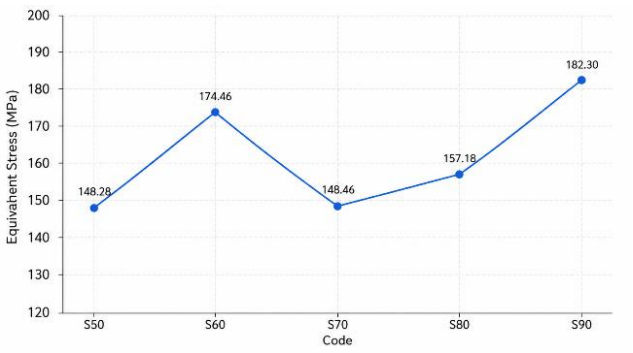
Fig. 9 Representative finite element results for the dBB configuration at S80



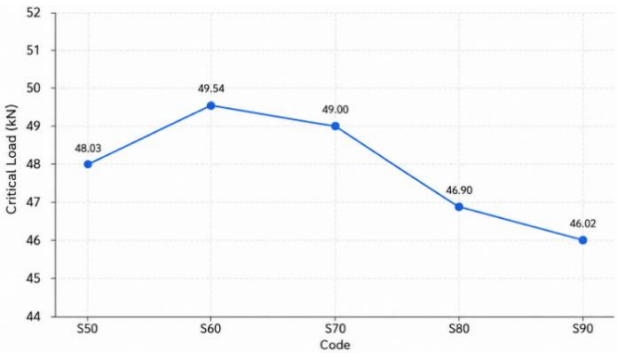

(a) Total deformation vs screw spacing




(b) Equivalent elastic strain vs screw spacing




(c) Equivalent stress vs screw spacing




(d) Critical load vs screw spacing

Fig .10 Numerical responses of the dBB configuration across the five overall screw distribution configurations

The first-mode elastic buckling shape at S80 shows predominantly local buckling. The deformation is concentrated in the thin-walled parts of the CFS profiles, without pronounced global flexural deformation of the complete column. This pattern indicates that the first elastic instability is associated mainly with local deformation of the profile elements. Because screw spacing and end distance vary simultaneously, changes in overall screw distribution may alter the interaction between the connected profiles and their local stiffness. Therefore, the response should be interpreted in relation to both connection distribution and the geometric characteristics of the dBB section.

Fig. 10 presents the numerical response for screw spacings of 50, 60, 70, 80, and 90 mm. The total deformation varies from 0.20548 mm at S60 to 0.20562 mm at S90, giving an absolute difference of 0.00014 mm, or approximately 0.07%. This negligible variation indicates that global elastic deformation is relatively insensitive to the investigated connection distributions under the applied 20 kN reference load. The fixed column length, profile geometry, material parameters, and number of screws provide consistent overall conditions for comparison. However, the small change in global deformation does not mean that the internal response and stability remain unchanged.

The equivalent elastic strain ranges from 0.00075514 at S50 to 0.00092358 at S90, corresponding to a variation of approximately 22.31%. The equivalent stress increases from 148.28 MPa at S50 to 182.30 MPa at S90, representing a variation of approximately 22.94%. Both parameters exhibit non-monotonic trends, with increases at S60, decreases at S70, and subsequent increases toward S90. This behavior suggests that the coupled changes in screw spacing and end distance influence internal stress and strain redistribution more strongly than global deformation. Since these two geometric parameters vary simultaneously, their individual effects cannot be separated in the present study.

For comparison with the adopted nominal compressive reference strength of 250 MPa, the maximum equivalent stress of 182.30 MPa corresponds to a stress utilization of 72.92% and a safety factor of approximately 1.37. The maximum equivalent elastic strain of 0.00092358 is approximately 77.21% of the theoretical compressive yield strain of 0.001196, calculated using the reference strength and Young's modulus of 209 GPa. These results indicate that the maximum calculated stress and strain remain below the adopted reference values under the applied load. Nevertheless, the increase in both parameters toward S90 indicates that internal structural response is more sensitive to the investigated connection distributions than global deformation.

The elastic buckling response exhibits a clearer variation across the configurations. The highest BLF occurs at S60, with a value of 2.4774 and a corresponding elastic eigenvalue buckling load of 49.54 kN. The lowest value occurs at S90, with a BLF of 2.3012 and a corresponding load of 46.02 kN. The 3.52 kN difference represents an approximately 7.11% reduction relative to the highest load. This result demonstrates that a nearly unchanged global deformation can coexist with a more noticeable change in relative elastic buckling stability. Within the investigated configurations, S60 provides the highest relative elastic buckling stability for dBB, but this finding should not be interpreted as a universal optimum screw spacing or a prediction of actual ultimate compression capacity.

The theoretical compressive yield strain was determined from the nominal compressive yield strength and Young's modulus. The equivalent elastic strain ranges from 0.00075514 at S50 to 0.00092358 at S90. The theoretical compressive yield strain was calculated as the ratio of the nominal compressive reference strength to Young's modulus, yielding 0.001196 for the adopted values of 250 MPa and 209 GPa. The maximum equivalent elastic strain at S90 corresponds to 77.21% of this reference strain. This result indicates that the maximum calculated strain remains below the adopted reference strain under the applied 20 kN load.

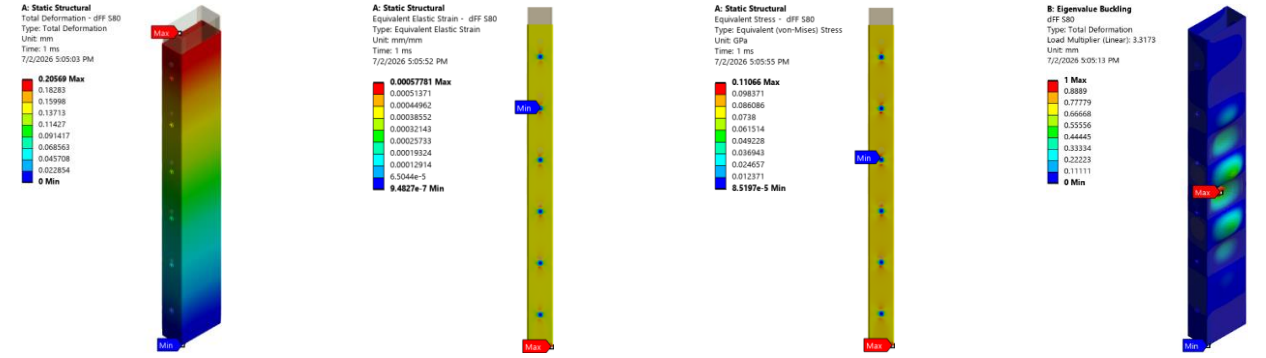
The equivalent stress values show a similar trend to the strain distribution. The maximum stress is obtained in the S90 configuration at 182.30 MPa, whereas the minimum value occurs in the S50 configuration at 148.28 MPa. The safety factor against yielding was determined from the ratio between the nominal yield strength and the maximum equivalent stress, as expressed by [22]:

$$SF = \frac{\sigma_y}{\sigma_{\max}} \tag{2}$$

The average equivalent stress is 162.14 MPa, with a stress range of 34.02 MPa. Based on the maximum stress of 182.30 MPa and the nominal yield strength of 250 MPa, the maximum stress utilization reaches 72.92%, corresponding to a safety factor of 1.37 against yielding. Therefore, the specimens remain within the nominal elastic range under the applied reference load of 20 kN, although the dBB configuration operates closer to the yield limit than the dFF configuration. The increase in stress toward the S90 configuration indicates a less uniform distribution of axial force within the built-up section.

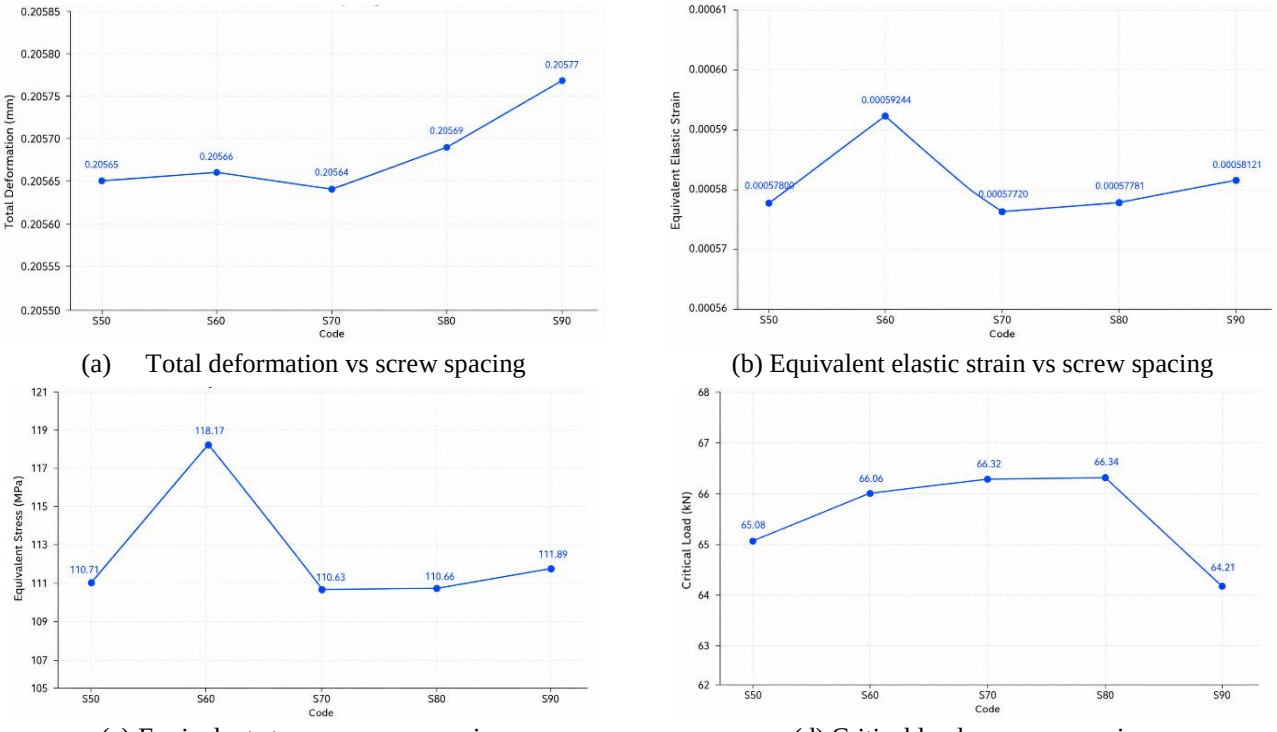
### *3.2 Structural response of double flange-to-flange configuration*

The numerical results for the dFF configuration are presented in Figs. 11 and 12. Fig. 11 shows the representative finite element results for S80, including total deformation, equivalent elastic strain, equivalent stress, and the first-mode elastic buckling shape. Fig. 12 presents the variations in these parameters across the five overall screw distribution configurations, with nominal screw spacings ranging from 50 to 90 mm. The numerical model and mesh sensitivity assessment are described in Section 2.3, while the experimental comparison for the S80 configuration is presented in Section 2.4.




(a) Total deformation (b) Equivalent elastic strain (c) Equivalent stress (d) First-mode elastic buckling shapes

Fig. 11 Representative finite element results for the dFF configuration at S80




(a) Total deformation vs screw spacing (b) Equivalent elastic strain vs screw spacing

(c) Equivalent stress vs screw spacing (d) Critical load vs screw spacing

Fig. 12 Numerical responses of the dFF configuration across the five overall screw distribution configurations

The first-mode elastic buckling shape at S80 shows predominantly local buckling. The deformation is distributed along the thin-walled connected profiles, while no clear global flexural deformation is observed. The distributed local deformation indicates that the first instability is governed primarily by the local response of the thin-walled profile elements rather than by global flexural buckling of the entire column. The dFF orientation provides a more symmetric arrangement of the two profiles, which may contribute to a more uniform structural response along the connected section. Consequently, changes in the overall screw distribution produce relatively small changes in the elastic buckling response compared with the dBB arrangement. The highest BLF of 3.3173 occurs at S80, corresponding to an elastic eigenvalue buckling load of 66.35 kN, whereas S90 gives the lowest BLF of 3.2106 and a corresponding load of 64.21 kN. The difference of 2.14 kN indicates that the investigated connection distributions modify elastic buckling stability, but the sensitivity remains limited within the dFF configuration.

The total deformation varies only slightly across the investigated configurations, ranging from 0.20564 to 0.20577 mm, corresponding to a maximum variation of only 0.00013 mm. This small variation indicates that the global elastic stiffness of the dFF arrangement remains nearly unchanged despite changes in the overall screw distribution. The equivalent elastic strain ranges from 0.00057720 to 0.00059244, giving a narrow variation of 0.00001524, while the equivalent stress varies from 110.63 to 118.17 MPa, corresponding to a stress difference of 7.54 MPa. The highest strain and stress occur at S60, whereas the lowest values occur at S70, indicating that the changes in connection distribution result in relatively limited redistribution of internal forces in the dFF arrangement. The maximum equivalent stress of 118.17 MPa corresponds to 47.27% of the nominal compressive yield strength of 250 MPa, giving a safety factor of 2.12 against yielding. Therefore, the investigated dFF configurations remain within the nominal elastic range, with the stress response showing substantially less variation than that observed for the dBB arrangement.

The elastic buckling response varies across the investigated connection distributions, but the variation remains relatively small compared with the dBB arrangement. The BLF increases from 3.2544 at S50 to 3.3173 at S80 before decreasing to 3.2106 at S90, indicating a nonlinear response to the coupled changes in screw spacing and end distance. The corresponding elastic eigenvalue buckling load increases from 65.09 kN at S50 to 66.35 kN at S80 and decreases to 64.21 kN at S90. The difference between the highest and lowest elastic buckling loads is 2.14 kN, equivalent to approximately 3.3% of the lowest value. This relatively narrow range indicates that the dFF configuration maintains a more consistent elastic buckling response across the investigated overall screw distributions. Within the investigated configurations, S80 provides the highest relative elastic buckling stability for the dFF arrangement.

## 4. Discussions

This section synthesizes the findings presented in Sections 3.1 and 3.2 to interpret the influence of overall screw distribution on the structural response and relative elastic buckling stability of built-up cold-formed steel columns. The discussion compares the sensitivity of the dBB and dFF configurations to changes in screw spacing and end distance, considering their different sectional properties and potential implications for internal force redistribution. Particular attention is given to the relationship between global deformation, stress and strain responses, and elastic buckling behavior. The discussion also addresses the limitations of the present analysis and the implications of the findings for evaluating the investigated connection configurations.

### *4.1 Effect of screw distribution on structural response*

The simulation results show that variations in screw distribution have different effects on each structural response parameter. These effects are relatively small for global deformation but more pronounced for strain and stress distributions. Differences in response are also influenced by the orientation of the profiles, indicating that the effects of variation in screw spacing differ between the dBB and dFF configurations.

In addition to the connection distribution, the orientation of the constituent profiles produces different geometric properties for the complete built-up sections. As shown in Table 2, the dBB and dFF arrangements exhibit different principal moments of inertia and radii of gyration, reflecting differences in their inherent sectional stiffness characteristics. These geometric characteristics, together with the connection distribution, contribute to the differences in structural and elastic buckling responses observed between the two configurations. Therefore, the comparison between the dBB and dFF arrangements should account for the combined influence of sectional geometry and connection distribution.

The results indicate that the overall screw distribution has a limited influence on global deformation. Both dBB and dFF configurations maintain nearly constant total deformation across the investigated cases. The total deformation varies by approximately 0.00014 mm in the dBB configuration and 0.00013 mm in the dFF configuration. This behavior suggests that the two CFS profiles continue to act as a combined structural system under the applied axial load.

A greater influence of the overall screw distribution is observed in the equivalent strain and stress responses. In the dBB configuration, the equivalent strain increases from 0.00075514 at S50 to 0.00092358 at S90, while the equivalent stress increases from 148.28 to 182.30 MPa. In comparison, the dFF configuration shows a narrower strain variation from 0.00057720 to 0.00059244 and a stress variation from 110.63 to 118.17 MPa. These results indicate that changes in the connection distribution produce a more pronounced redistribution of internal forces in the dBB arrangement than in the dFF arrangement. Because increasing screw spacing simultaneously reduces the end distance, the connected and unconnected regions along the column change together, thereby potentially modifying the path through which axial forces are transferred between the two profiles. The larger strain and stress variations in the dBB configuration suggest that its force-transfer mechanism is more sensitive to these changes in connection distribution. In contrast, the smaller variations in the dFF configuration indicate a more uniform redistribution of internal forces, which may be associated with its different assembled sectional characteristics.

Overall, the results indicate that changes in connection distribution influence internal force redistribution more noticeably than global elastic deformation. The dBB configuration exhibits a strain range of 0.00016844 and a stress range of 34.02 MPa, whereas the corresponding ranges for dFF are only 0.00001524 and 7.54 MPa. These differences demonstrate that the dBB arrangement is more sensitive to changes in overall connection distribution, while the dFF arrangement maintains a comparatively more uniform elastic response.

### *4.2 Effect of screw distribution on buckling behavior*

The discussion in this section is limited to the relative elastic buckling response obtained from the linear eigenvalue analysis. Accordingly, differences in BLF and the corresponding elastic eigenvalue buckling loads are interpreted as indicators of relative buckling stability among the investigated configurations. These results should not be interpreted as direct predictions of the actual ultimate compression capacity because geometric imperfections, material nonlinearity, large deformation, connection slip, and post-buckling behavior are not explicitly included in the present analysis.

The first eigenmodes obtained for the investigated configurations are predominantly local buckling modes. The deformation is concentrated in the thin-walled plate elements of the built-up profiles, while no dominant global flexural buckling pattern is observed. Therefore, the differences in BLF among the configurations are interpreted primarily in relation to changes in the local stability of the assembled thin-walled section and the interaction between the connected profiles.

The corrected stress results further support this limitation. Under the reference load of 20 kN, the maximum equivalent stress in the dBB configuration reaches 182.30 MPa, corresponding to approximately 72.92% of the nominal yield strength. Therefore, a direct linear scaling of the elastic stress state by the eigenvalue buckling load factor would lead to stress levels exceeding the nominal yield strength. This confirms that the eigenvalue buckling load should not be interpreted as an ultimate compression capacity. Accordingly, the BLF is used only to compare the relative elastic buckling stability of the configurations.

The elastic buckling response is more sensitive to the overall screw distribution than the global deformation response. In the dBB configuration, the BLF increases from 2.4018 at S50 to 2.4774 at S60 before decreasing to 2.3012 at S90. The corresponding elastic eigenvalue buckling load increases from 48.03 kN to 49.54 kN and then decreases to 46.02 kN. Thus, the difference between the highest and lowest critical loads is 3.52 kN, indicating a measurable variation in relative elastic buckling stability across the investigated connection distributions. The non-monotonic trend indicates that the coupled changes in screw spacing and end distance modify the balance between connected and unconnected regions along the column. This behavior suggests that the elastic stability of the dBB configuration may depend on how the connection distribution affects the interaction between the two profiles.

In the dFF configuration, the BLF increases from 3.2544 at S50 to a maximum of 3.3173 at S80 before decreasing to 3.2106 at S90. The corresponding elastic eigenvalue buckling load varies from 65.09 kN at S50 to 66.35 kN at S80 and decreases to 64.21 kN at S90. The difference between the highest and lowest critical loads is 2.14 kN, which is smaller than the 3.52 kN variation observed in the dBB configuration. This narrower range indicates that the elastic buckling response of the dFF arrangement is less sensitive to the investigated changes in overall screw distribution. The reduction in BLF from S80 to S90 further shows that increasing the screw spacing beyond the investigated S80 configuration does not continuously improve relative elastic buckling stability.

The difference between the dBB and dFF responses is also associated with their sectional characteristics. The two assemblies have different principal moments of inertia and radii of gyration, which affect the stiffness and stability of the complete built-up sections. These geometric characteristics interact with the screw distribution and may influence the transfer of compressive force between the connected profiles. Because the first eigenmodes are predominantly local, the observed differences in BLF are therefore related primarily to local stability and profile interaction, rather than dominant global flexural buckling.

Within the investigated range of connection distributions, the dBB configuration attains its highest relative elastic buckling stability at S60, whereas the dFF configuration reaches its highest value at S80. These findings describe the relative elastic response obtained from the present eigenvalue analysis and should not be interpreted as universal optimum configurations. A more complete assessment of buckling resistance would require nonlinear analyses that incorporate initial geometric imperfections, material nonlinearity, large deformation, connection slip, and post-buckling behavior.

## 5. Conclusions

This study investigated five overall screw distribution configurations (S50–S90) in built-up cold-formed steel (CFS) columns with a fixed length of 500 mm and six self-drilling screws. Double back-to-back (dBB) and double flange-to-flange (dFF) arrangements were evaluated using Static Structural and linear Eigenvalue Buckling analyses. Because screw spacing and end distance varied simultaneously, the findings represent the combined effect of overall screw distribution rather than isolated screw spacing. Based on these analyses, the main conclusions are summarized as follows:

(1) The overall screw distribution has a negligible effect on global elastic deformation. The deformation range was 0.20548–0.20562 mm for dBB and 0.20564–0.20577 mm for dFF, corresponding to variations of approximately 0.07% and 0.06%, respectively. The maximum absolute changes were only 0.00014 mm for dBB and 0.00013 mm for dFF under the applied 20 kN reference load. Accordingly, global deformation alone provides limited differentiation among the investigated connection configurations.

(2) The sensitivity of internal strain and stress differs substantially between the two profile orientations. For dBB, equivalent elastic strain ranged from 0.00075514 to 0.00092358, representing a variation of 22.31%, while equivalent stress ranged from 148.28 to 182.30 MPa, representing a variation of 22.94%. For dFF, the corresponding strain and stress variations

were only 2.64% and 6.82%, respectively. These results demonstrate that internal strain and stress in dBB are more sensitive to changes in overall screw distribution than those in dFF.

(3) In terms of the buckling load factor (BLF), the difference between the highest and lowest values was 0.1762 for dBB and 0.1067 for dFF. These differences correspond to approximately 7.11% and 3.22% of the respective highest BLF values. The associated elastic eigenvalue buckling loads varied by 3.52 kN for dBB and 2.14 kN for dFF. These variations show that relative elastic buckling stability is more responsive to the investigated configurations than global elastic deformation.

(4) The highest relative elastic buckling stability occurred at S60 for dBB and S80 for dFF, with BLFs of 2.4774 and 3.3173, respectively. Their corresponding elastic eigenvalue buckling loads were 49.54 and 66.35 kN. The different configurations demonstrate that the highest BLF depends on the assembled profile orientation. These configurations represent the highest relative elastic buckling stability only within the investigated range and do not establish universal optimum screw spacing values.

(5) The applicability of these findings is limited to the investigated 500 mm columns, six-screw arrangement, five screw spacings of 50–90 mm, and corresponding end distances of 125–25 mm. Because screw spacing and end distance were varied simultaneously, their individual contributions cannot be isolated from the present results. Furthermore, the experimental comparison was limited to the S80 configurations, while the parametric study relied on linear-elastic analysis and eigenvalue buckling. Consequently, the present results support comparisons of elastic response and relative buckling stability but do not establish actual ultimate compression capacity. Further investigation using geometrically and materially nonlinear analysis with initial imperfections and connection behavior is required to assess ultimate capacity and post-buckling response.

## Acknowledgment

This study is financially supported by the research program of the University of Muhammadiyah Malang (UMM), Indonesia. The authors gratefully acknowledge the university's financial support, which made this research possible.

## Conflicts of Interest

The authors declare no conflict of interest.

## References

[1] X. Zou, Y. Zhu, and L. Zhang, "A Decade of Developments in the Mechanical Performance of Cold-Formed Steel Members," Mechanics of Solids, vol. 61, no. 2, article no. 89, 2026.

[2] H. Hendaryati, A. F. H. Soegiharto, R. D. Virdianto, and A. Saifullah, "Analysis of the Effect of Cooling Media Variations on Tensile Strength of Electrical Welding Results of S45C Steel," AIP Conference Proceedings, vol. 2453, no. 1, article no. 020004, 2022.

[3] M. A. Dar, S. A. Baba, M. Zakir, and A. R. Dar, "Flexural Performance of Sustainably Composite-Stiffened Cold-Formed Steel Built-Up Beams with Rectangular Compression Flanges," The Structural Design of Tall and Special Buildings, vol. 35, no. 2, article no. e70130, 2026.

[4] D. B. Hussein and A. B. Hussein, "Investigating the Factors Influencing the Strength of Cold-Formed Steel (CFS) Sections," Buildings, vol. 14, no. 4, article no. 1127, 2024.

[5] N. Kharghani and C. Mittelstedt, "Global–Local–Distortional Buckling of Shear-Deformable Composite Beams with Open Cross-Sections Using a Novel GBT–Ritz Approach," Journal of Composites Science, vol. 9, no. 11, article no. 608, 2025.

[6] N. Subeki, A. F. H. Soegiharto, A. Firkriyanto, and N. Gidiazalia, "Crack Propagation Analysis of Fatigue Due to External Corrosion on the Construction of the Ferris Wheel in Alun-Alun Kota Batu," Journal of Advanced Research in Applied Mechanics, vol. 111, no. 1, pp. 62–73, 2023.

[7] M. Elsawi Mahmoud, A. El-Sisi, A. Elbelbisi, H. Elemam, and H. Salim, "Performance of CFS Trusses Self-Drilling Screws Connections Under Extreme Loads," Structures, vol. 74, article no. 108592, 2025.

[8] J. Yang, K. Luo, W. Wang, Y. Shi, and H. Li, "Research on the Flexural Buckling Behavior of the Cold-Formed Steel Back-to-Back Built-Up Columns with Σ-Section," Engineering Structures, vol. 302, article no. 117404, 2024.

[9] S. T. Vy and M. Mahendran, "Screwed Connections in Built-Up Cold-Formed Steel Members at Ambient and Elevated Temperatures," Journal of Constructional Steel Research, vol. 192, article no. 107218, 2022.

[10] N. Soysal and Z. Fırat Alemdar, "Numerical and Experimental Assessment of Structural Performance and Axial Compression Capacity of Screw-Connected Built-Up Cold-Formed Steel Members," Buildings, vol. 16, no. 9, article no. 1651, 2026.

[11] H. Wu, L. Sui, X. Liu, S. Liang, and T. Zhou, "Shear-Slip Constitutive Model of Screw-Fastened Connections and Application in Numerical Analysis of Built-Up Back-to-Back Cold-Formed Steel Columns," Thin-Walled Structures, vol. 186, article no. 110710, 2023.

[12] Z. Septiropa, M. H. Osman, A. B. A. Rahman, and M. A. M. Ariffin, "Effect of Screw Distance on Combined Profiles Cold-Formed Steel in Increasing the Compression Member Capacity," IOP Conference Series: Materials Science and Engineering, vol. 527, no. 1, article no. 012080, 2019.

[13] P. Deniziak, E. Urbańska-Galewska, and M. Gordziej-Zagórowska, "Normal Stress Distribution in Built-Up Cold-Formed Column in Relation to Interconnecting Bolt Spacing," Scientific Reports, vol. 14, no. 1, article no. 5415, 2024.

[14] M. B. Suhaib and M. A. Tantray, "Flexural Integrity Between the Individual Channels of Built-Up Cold-Formed Steel Beams," International Journal of Steel Structures, vol. 23, no. 2, pp. 503–520, 2023.

[15] J. Feron, P. Latteur, and J. Pacheco de Almeida, "Static Modal Analysis: A Review of Static Structural Analysis Methods Through a New Modal Paradigm," Archives of Computational Methods in Engineering, vol. 31, no. 6, pp. 3409–3440, 2024.

[16] M. N. Bin Kamarudin, J. S. Mohamed Ali, A. Aabid, and Y. E. Ibrahim, "Buckling Analysis of a Thin-Walled Structure Using Finite Element Method and Design of Experiments," Aerospace, vol. 9, no. 10, article no. 541, 2022.

[17] A. B. Hussein, "Structural Behaviour of Built-Up I-Shaped CFS Columns," Scientific Reports, vol. 14, no. 1, article no. 25628, 2024.

[18] K. Mitsui, A. Sato, and K. Ikarashi, "Required Number of Self-Drilling Screws for Built-Up Column Comprising Cold-Formed Lipped Channel Sections to Ensure Flexural Buckling as a Single Unit Member," Japan Architectural Review, vol. 6, no. 1, article no. e12354, 2023.

[19] M. Abbasi, K. J. R. Rasmussen, M. Khezri, and B. W. Schafer, "Computational Modelling of Built-Up Cold-Formed Steel Columns and Parametric Studies," Thin-Walled Structures, vol. 191, article no. 111035, 2023.

[20] F. De'nan, K. K. Choong, J. Y. Ling, and N. S. Hashim, "Finite Element Analysis of Buckling Behavior for Cold-Formed Steel Hat Purlins with Openings," International Journal of Steel Structures, vol. 22, no. 4, pp. 982–1001, 2022.

[21] J. He and B. Young, "Web Crippling Design of Cold-Formed Steel Built-Up I-Sections," Engineering Structures, vol. 252, article no. 113731, 2022.

[22] M. Amjad, S. Badshah, S. Ahmad, M. Badshah, S. Jan, M. Yasir, et al., "Finite Element Modeling of Stress Distribution and Safety Factors in a Ti-27Nb Alloy Hip Implant Under Real-World Physiological Loading Scenarios," PLoS ONE, vol. 19, no. 8, article no. e0300270, 2024.



Copyright© by the authors. Licensee TAETI, Taiwan. This article is an open access article distributed under the terms and conditions of the Creative Commons Attribution (CC BY-NC) license (https://creativecommons.org/licenses/by-nc/4.0/).